Electronic Supporting Information

Extraordinary thermoelectric performance of NaBaBi with degenerate and highly non-parabolic bands compared to LiBaSb and Bi_2Te_3

Enamul Haque
EH Solid State Physics Laboratory, Longaer, Gaffargaon-2233, Mymensingh, Bangladesh.
Email: enamul.phy15@yahoo.com

S1. Computational Details

In this study, I used a set of first-principles codes to calculate the different types of properties. First I performed structural relaxation by using the plane wave method as implemented in Quantum Espresso [1]. In the calculation, I set a very strict convergence criterion (energy convergence 10^{-14} Ry, force 0.1 mRy/au and Pulley stress 0.1 kbar) to obtain the ground state structure. The exchange-correlation part was treated through generalized gradient approximation (GGA) with PBEsol setting by using PAW [2] pseudopotential for Bi_2Te_3 and ultrasoft Vanderbilt [3] for NaBaBi and LiBaSb. I selected 41.52, 48.5, and 55.5 Ry cutoff energy for wavefunction, 166, 194, and 222 Ry for charge density and, $6 \times 6 \times 6$, $6 \times 6 \times 10$, $8 \times 8 \times 4$ Γ-centered k-point with Marzari-Vanderbilt smearing [4] of width 0.03 Ry after extensive trials. Since the electron-phonon matrix calculation is very expensive, I used 444, 444, and 442 uniform q-point grids (and $8 \times 8 \times 8, 8 \times 8 \times 12, 12 \times 12 \times 6$ k-point mesh) to reduce the computational burden. The average electron-phonon dynamical matrix was calculated by using EPA code [5]. The numbers of energy bins used in these calculations were 10, 6, and 8 after extensive trials.

The use of relatively loose q-point might have a slight negative impact on the accuracy of the electron-phonon scattering matrix. To check this impact, the calculations of the average e-ph matrix were repeated by using a moving least square method (MLS) [6] with 30 energy bins for each compound, which is less sensitive (even it allows to use of 222 q-point grid without the loss of significant accuracy) to the q-point grid and found negligible impact. The matrix was then fed into slightly modified BoltzTraP [7] code to calculate transport coefficients. This code uses the semiclassical Boltzmann transport theory and thus, requires accurate electronic structure calculations. To calculate accurate electronic structure, I used Tran-Blah modified Becke-Johnson potential[8], as implemented in wien2k, a full-potential linearized augmented plane wave method based code [9,10]. To proceed with this calculation, I first minimized the atomic forces again in Wien2k by using PBEsol, with the same k-point, plane-wave cutoff RK_{max}=7, valence and core state separation energy -10.0 for Bi_2Te_3, and -6.0 Ry for NaBaSb and LiBaSb, muffin tin sphere radii 1.96 Bohr for Bi and Te, 2.1 and 2.3 Bohr for Na and Ba/Bi, 2.19 and 2.5 Bohr for Li and Ba/Sb, respectively. I then performed the electronic structure calculation by using a denser $32 \times 32 \times 32$, $30 \times 30 \times 43$, and $44 \times 44 \times 21$ non-shifted k-point mesh to obtain energy eigenvalues. In the electronic structure and transport calculations, I included the spin-orbit

coupling (SOC) effect with upper window energy 8.0 Ry explicitly by performing fully-relativistic calculations.

I calculated the lattice thermal conductivity (κ_l) by using 221, 112, and 221 supercells for Bi_2Te_3, NaBaBi, and LiBaSb, respectively, as implemented in phono3py [11]. To calculate, second-order and third-order interatomic force constants (IFCs), the force calculations were performed in QE (with the same setting as before, except for k-point, in this case $2 \times 2 \times 2$ k-point mesh was used.) for each displacement. Note this type of calculation is very expensive and spin-orbit coupling has little effect on the lattice thermal conductivity, so this effect was not included in the force calculations. After the force calculations, κ_l was obtained by solving the linear Boltzmann phonon equation with $16 \times 16 \times 16$ q-point. Note that q-point convergence was also checked by using a set of different q-points. In the κ_l calculation, I used the relaxation time approximation (RTA) in Phono3Py as the full scattering operator requires to calculate the full collision matrix, which is very expensive. Fortunately, the experimental value of κ_l of Bi_2Te_3 is available and I repeated the calculation of κ_l for Bi_2Te_3 only by using the full scattering operator with the tetrahedron method for integration. This method was found to underestimate the experimental value of κ_l further, although the difference, between the values of κ_l obtained by this method and RTA, is less than 1%. I also verified the κ_l calculation of NaBaBi by using full iterative solutions of the phonon Boltzmann transport equation as implemented in ShengBTE [12] (by performing the force constants calculations with the same settings as that for Phono3Py) and found almost the same results. In other cases, the calculations were not repeated as these are very expensive.

S2. Lattice dynamics

The computed group velocity and mode Grüneisen parameter of these compounds are shown in Fig. S1 and Fig. S2, respectively. The group velocity of acoustic phonons of NaBaBi is almost similar to that of Bi_2Te_3 while the group velocity of optical phonons of NaBaBi is much slower than that of Bi_2Te_3. Thus, the optical phonons with energy above 3 THz of NaBaBi have a negligible contribution to the heat conduction while the contributions of these phonons of Bi_2Te_3 cannot be neglected.

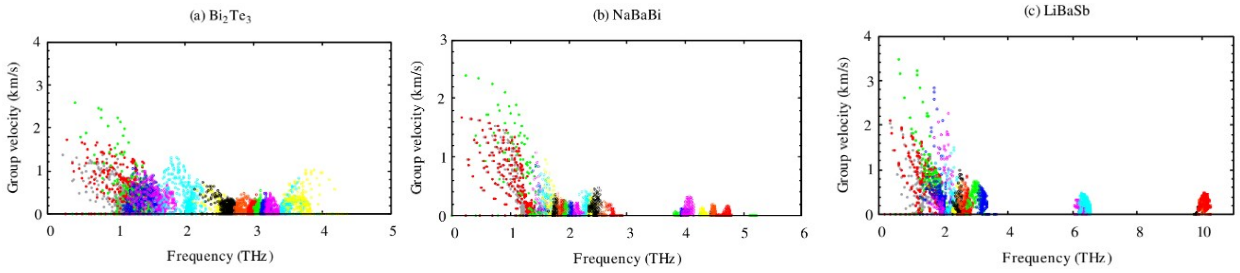

Fig. S1. Computed phonon group velocity of (a) Bi_2Te_3, (b) NaBaBi, and (c) LiBaSb from second-order harmonic IFCs.

In comparison to the former two compounds, the group velocity of acoustic phonons of LiBaSb is much larger. The mode Grüneisen parameter (mGp) of three acoustic phonons (light gray, red, and green colored circles in Fig. S2) of NaBaBi and Bi_2Te_3 shows a similar trend. The mGp of these two compounds expand over the positive and negative values, unlike that of LiBaSb.

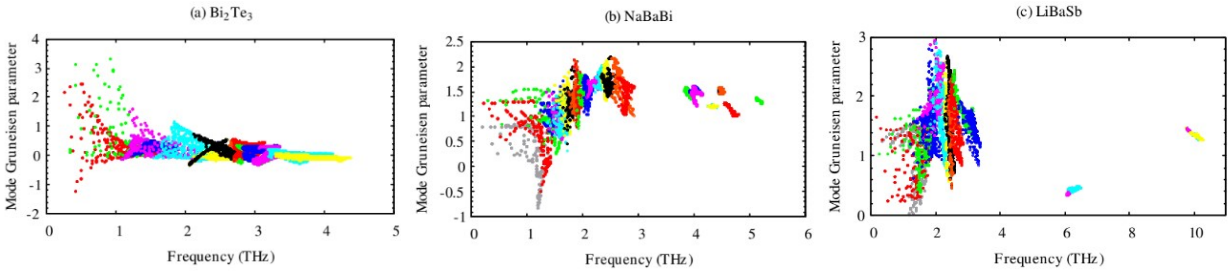

Fig. S2. Mode Grüneisen parameter of (a) Bi_2Te_3, (b) NaBaBi, and (c) LiBaSb calculated from anharmonic IFCs.

The optical phonons with energy 1-3 THz of NaBaBi have much larger values of mGp as compared to that of Bi_2Te_3. Although these optical phonons of LiBaSb have larger values of mGp, most of the heat is conducted through acoustic phonons of this compound. Similar values of the group velocity and mGp of acoustic phonons of NaBaBi relative to the Bi_2Te_3 suggest that the heat conduction would also be similar.

S3. Carrier transport

Fig. S3 shows the energy dependence anisotropic carrier lifetime of the studied compounds at three consecutive temperatures. The zero-energy represents the Fermi level.

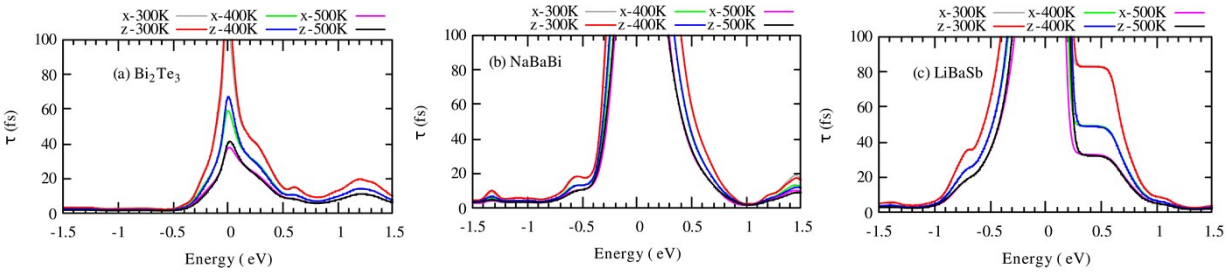

Fig. S3. Energy-dependent anisotropic carrier lifetime (τ) at three consecutive temperatures of (a) Bi_2Te_3, (b) NaBaBi, and (c) LiBaSb. The Fermi level was set to zero.

From Fig. S3, it is clear that the low density of states near the Fermi level leads to a longer lifetime and vice versa. The widest bandgap and lowest density of states near the Fermi level of LiBaSb compared to other studied compounds lead to the longest carrier lifetime. The computed absolute

anisotropic thermopower (Seebeck coefficient (S)) also shows the same trend, as shown in Fig. S4.

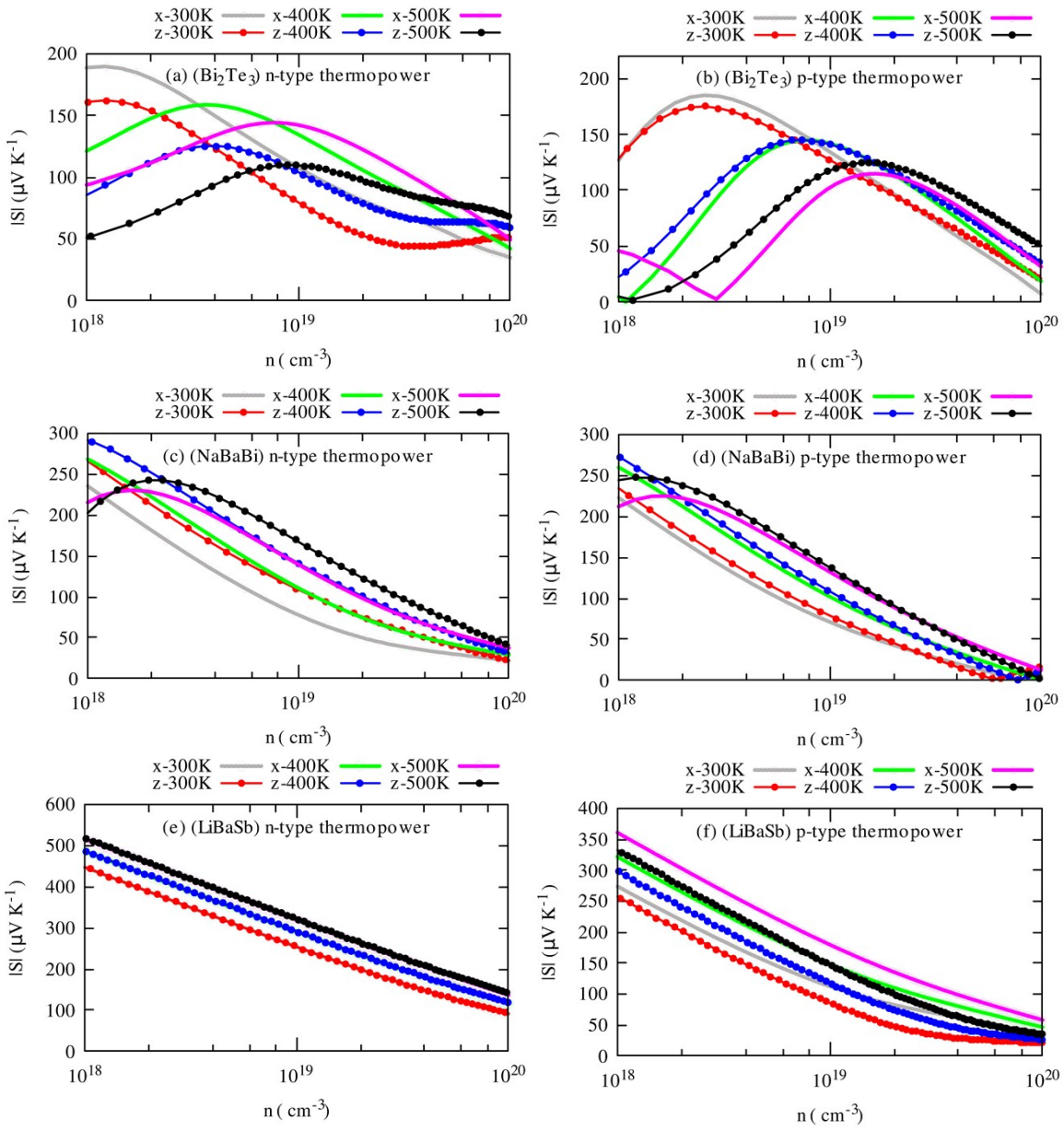

Fig. S4. Carrier concentration dependent absolute values of in-plane (*x*) and cross-plane (*z*) thermopower of (a-b) Bi_2Te_3, (c-d) NaBaBi, and (e-f) LiBaSb for *n*- and *p*-type carriers at three consecutive temperatures.

Although the thermopower of Bi_2Te_3 and NaBaBi exhibits anisotropic behavior, the thermopower of LiBaSb exhibits isotropic for electrons and slightly anisotropic for holes over the studied carrier concentration limit.

The anisotropic electrical conductivities (σ) of Bi_2Te_3, NaBaBi, and LiBaSb as a function of carrier concentration at three consecutive temperatures are shown in Fig. S5.

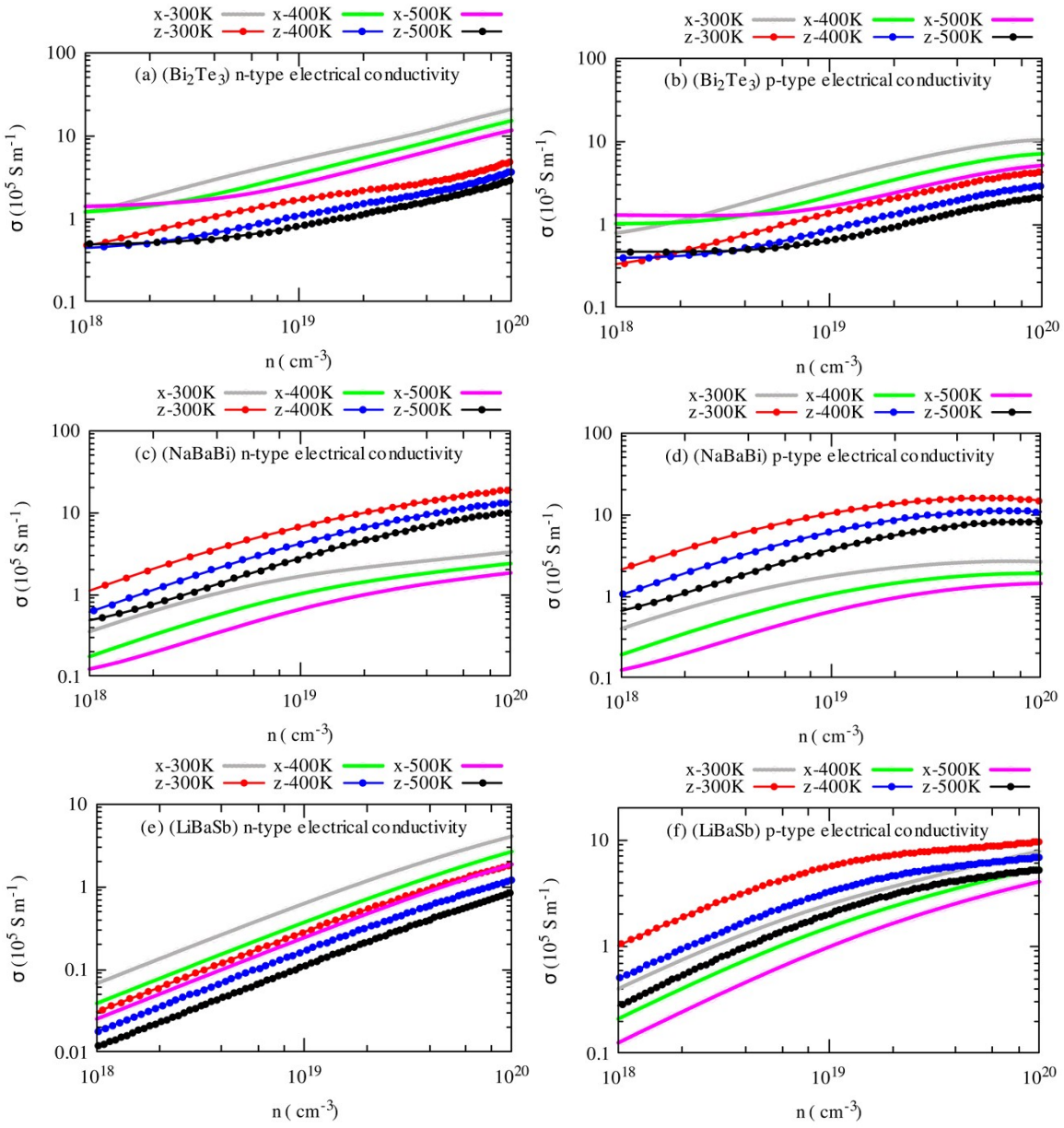

Fig. S5. Carrier concentration dependent in-plane (*x*) and cross-plane (*z*) electrical conductivity of (a-b) Bi_2Te_3, (c-d) NaBaBi, and (e-f) LiBaSb for *n*- and *p*-type carriers at three consecutive temperatures.

Unlike thermopower, the electrical conductivity sharply rises with carrier density and shows anisotropic behavior. The electrical conductivity of Bi_2Te_3 more slowly changes with carrier density due to its inherent high carrier density compared to NaBaBi and LiBaSb. By using the

thermopower and electrical conductivity, the power factor ($PF=S^2\sigma$) has been calculated along with the crystallographic directions and shown in Fig. S6.

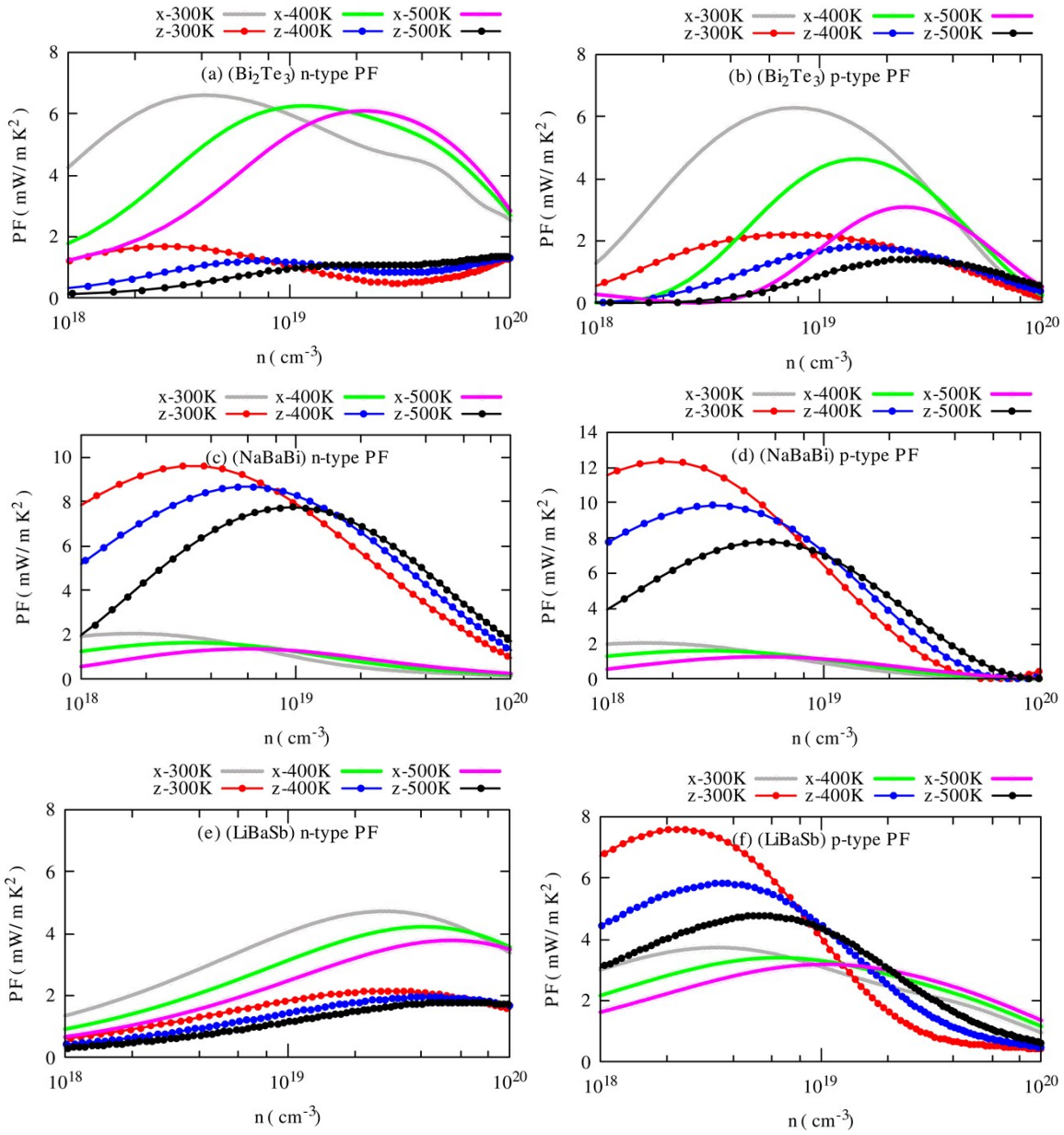

Fig. S6. Calculated in-plane (x) and cross-plane (z) power factor as a function of carrier concentration of (a-b) Bi_2Te_3, (c-d) NaBaBi, and (e-f) LiBaSb for n- and p-type carriers at three consecutive temperatures.

NaBaBi has the largest anisotropic power factor for both electrons and holes compared to the other studied compounds. The power factor of Bi_2Te_3, NaBaBi, and p-type LiBaSb shows highly

anisotropic behavior below $10^{19}\ cm^{-3}$ and weakly anisotropic above $10^{19}\ cm^{-3}$. However, the *PF* of *n*-type LiBaSb exhibits isotropic behavior over the studied carrier concentration due to its isotropic thermopower. The anisotropic power factor of the studied compounds as a function of temperature at a fixed carrier density (listed in Table III, see in the main text) are shown in Fig. S7.

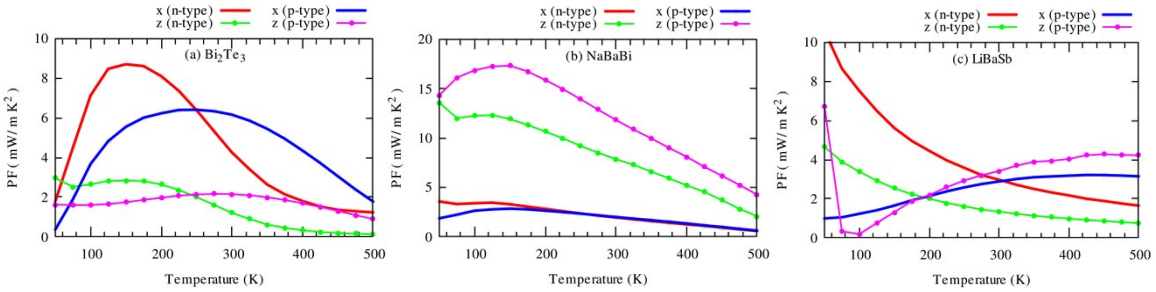

Fig. S7. Temperature dependent anisotropic power factor of (a) Bi_2Te_3, (b) NaBaBi, and (c) LiBaSb.

The *PF* becomes maximum below 200 K in all cases except *n*-type LiBaSb, in which it sharply rises with temperature. This might be due to the wider bandgap and weak response of the effective mass of electrons to the temperature. Within the studied temperature range, the cross-plane power factor of NaBaBi is dominated over that of the other studied compounds.

Fig. S8 shows the carrier concentration-dependent electronic part of the anisotropic thermal conductivity (κ_e) at three consecutive temperatures. The κ_e of NaBaBi for both electrons and holes is much smaller compared to that of Bi_2Te_3 below $10^{19}\ cm^{-3}$, due to the low density of states near the Fermi level. Above $10^{19}\ cm^{-3}$, the cross-plane κ_e of NaBaBi is higher for holes and comparable for electrons relative to in-plane κ_e of Bi_2Te_3. However, the in-plane κ_e of NaBaBi remains comparable to the cross-plane κ_e of Bi_2Te_3 over the studied carrier concentration range.

On the other side, LiBaSb has the lowest κ_e for electrons compared to other compounds. This can be understood from the calculated total density of states (DOS) (see Fig. 6 in the main text). The DOS of the conduction bands near the Fermi level of LiBaSb has the lowest value compared to that of Bi_2Te_3 and NaBaBi. However, the DOS of valence bands near the Fermi level is much higher compared to the conduction bands leading to higher *p*-type κ_e.

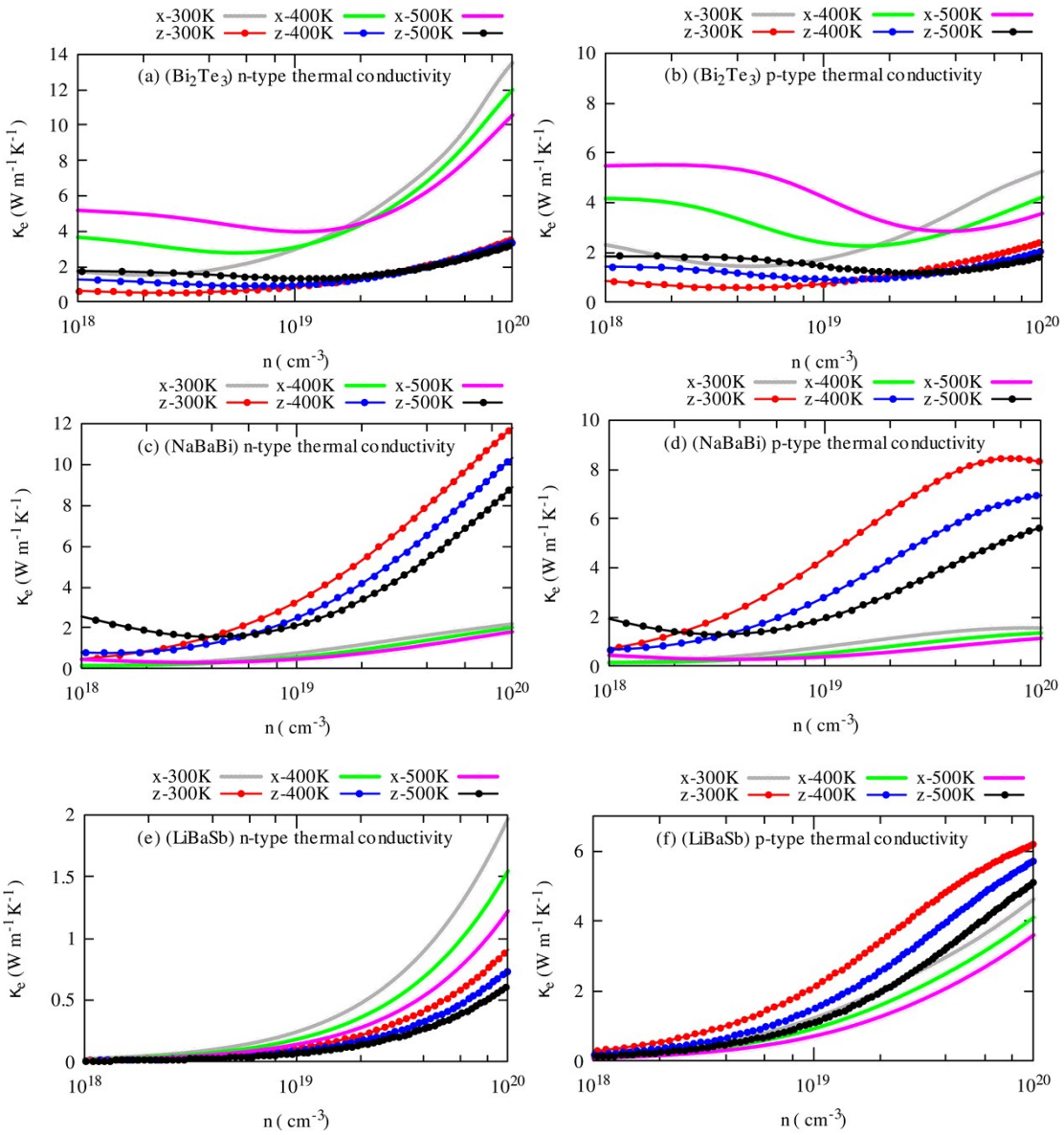

Fig. S8. Carrier concentration dependency of in-plane (x) and cross-plane (z) electronic part of the thermal conductivity of (a-b) Bi_2Te_3, (c-d) NaBaBi, and (e-f) LiBaSb for n- and p-type carriers at three consecutive temperatures.

Therefore, the low value of κ_e of NaBaBi near optimum carrier concentration will boost the thermoelectric performance further.

S4. Thermoelectric performance

From the calculated thermopower, electrical conductivity, and total thermal (electronic plus phononic contribution), the anisotropic thermoelectric figure of merit (*ZT*) is extracted and presented in Fig. S9. The *ZT* shows highly anisotropic behavior at certain carrier concentration in all cases. The *ZT* of Bi_2Te_3 is maximum along in-plane while the *ZT* of NaBaBi is maximum along cross-plane because these two compounds have opposite structural anisotropy.

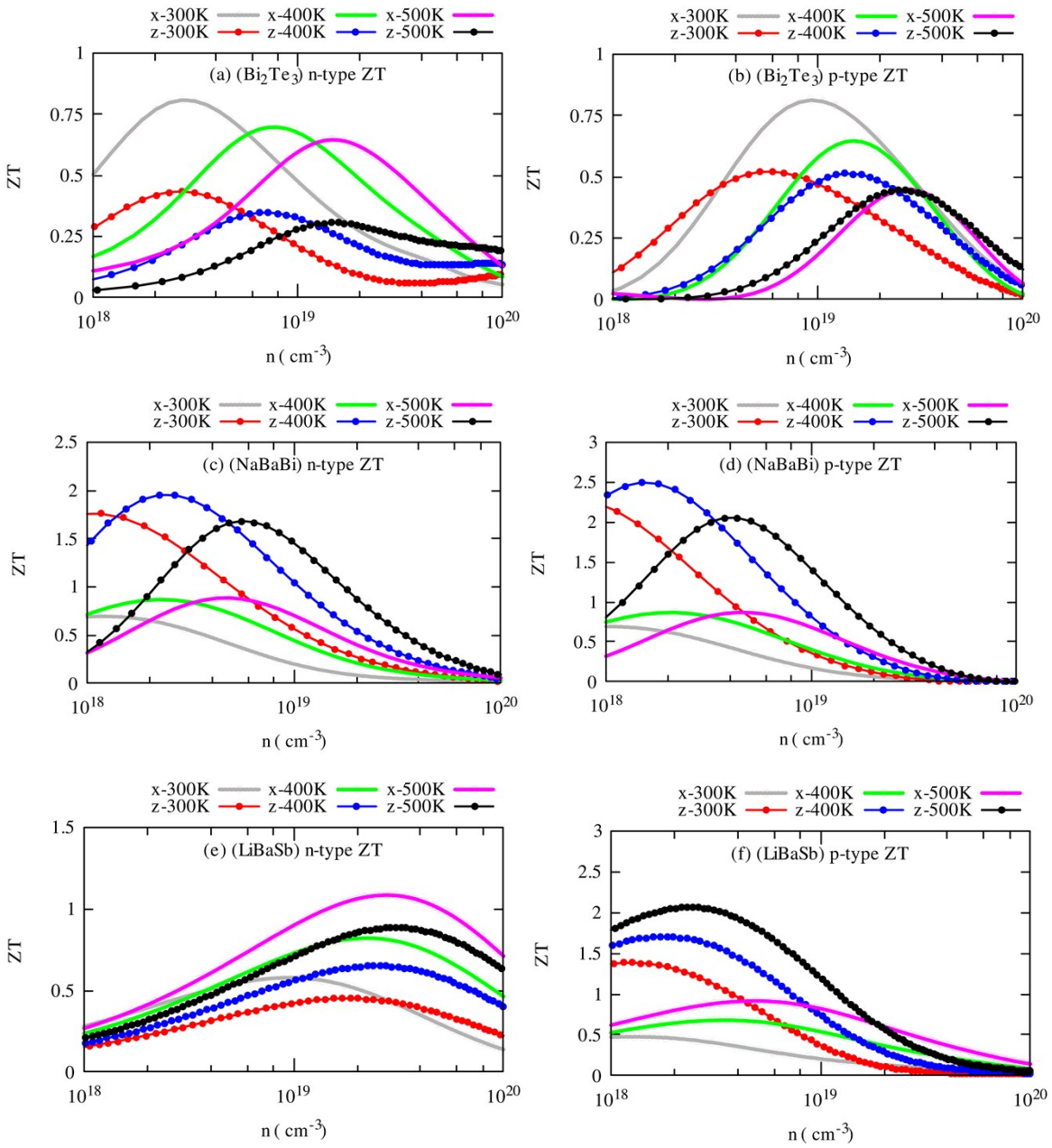

Fig. S9. Predicted anisotropic thermoelectric figure of merit as a function of a carrier concentration of (a-b) Bi_2Te_3, (c-d) NaBaBi, and (e-f) LiBaSb for *n*- and *p*-type carriers at three consecutive temperatures.

Like NaBaBi, the cross-plane *ZT* of LiBaSb is maximum and can reach ~1 and 2 for electrons and holes at 500 K. NaBaBi has the largest *ZT* for both *n*- and *p*-type carriers among these compounds. The cross-plane *ZT* can reach up to ~2 and 2.5 at 400 K for *n*- and *p*-type carriers, respectively. But in-plane *ZT* remains below one for both types of carriers. However, the *ZT* of Bi_2Te_3 remains below one for both types of carriers and crystallographic directions.

Fig. S10 shows the temperature effect on the anisotropic thermoelectric figure of the studied compounds. The *ZT* of Bi_2Te_3 becomes maximum at 200 K, while it is maximum at 350 K in the case of NaBaBi due to its wider bandgap.

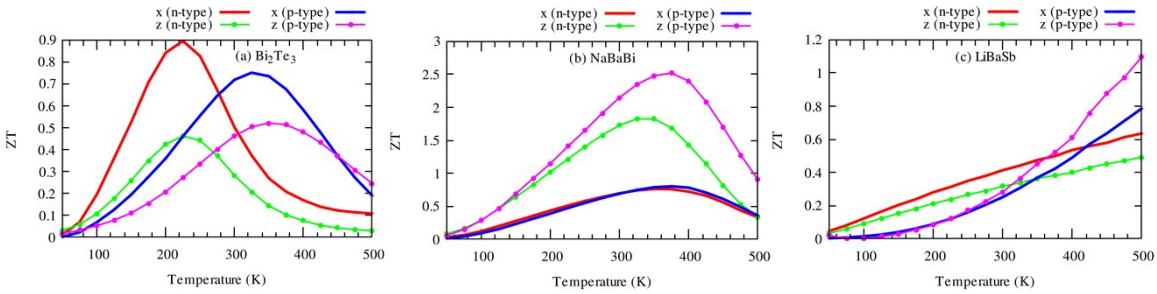

Fig. S10. Computed temperature-dependent anisotropic figure of merit (ZT) of (a) Bi_2Te_3, (b) NaBaBi, and (c) LiBaSb.

On the other side, the *ZT* of LiBaSb sharply rises with temperature suggesting that its potential thermoelectric performance at medium range temperature. The room temperature *ZT* of it is much smaller for *p*-type carriers than that of *p*-type Bi_2Te_3, but close for n-type carriers to that of *n*-type Bi_2Te_3. Therefore, LiBaSb is less suitable material for thermoelectric device applications considering the computational uncertainty and widest bandgap of LiBaSb.

References

1 P. Giannozzi, S. Baroni, N. Bonini, M. Calandra, R. Car, C. Cavazzoni, D. Ceresoli, G. L. Chiarotti, M. Cococcioni, I. Dabo and others, *J. Phys. Condens. matter*, 2009, **21**, 395502.

2 A. Dal Corso, *Comput. Mater. Sci.*, 2014, **95**, 337–350.

3 D. Vanderbilt, *Phys. Rev. B*, 1990, **41**, 7892.

4 N. Marzari, D. Vanderbilt, A. De Vita and M. C. Payne, *Phys. Rev. Lett.*, 1999, **82**, 3296.

5 G. Samsonidze and B. Kozinsky, *Adv. Energy Mater.*, 2018, **8**, 1800246.

6 S. Bang, J. Kim, D. Wee, G. Samsonidze and B. Kozinsky, *Mater. Today Phys.*, 2018, **6**, 22–30.

7 G. K. H. Madsen and D. J. Singh, *Comput. Phys. Commun.*, 2006, **175**, 67–71.

8 F. Tran and P. Blaha, *Phys. Rev. Lett.*, 2009, **102**, 226401.

9 P. Blaha, K. Schwarz, G. K. H. Madsen, D. Kvasnicka, J. Luitz, R. Laskowski, F. Tran and L. D. Marks, *WIEN2k, An Augmented Plane Wave + Local Orbitals Program for Calculating Crystal Properties (Karlheinz Schwarz, Techn. Universität Wien, Austria)*, ISBN 3-9501031-1-2, 2018.

10 P. Blaha, K. Schwarz, F. Tran, R. Laskowski, G. K. H. Madsen and L. D. Marks, *J. Chem. Phys.*, 2020, **152**, 74101.

11 A. Togo, L. Chaput and I. Tanaka, *Phys. Rev. B*, 2015, **91**, 94306.

12 W. Li, J. Carrete, N. A. Katcho and N. Mingo, *Comput. Phys. Commun.*, 2014, **185**, 1747–1758.